IET Image Processing

Research Article

IET Journals
The Institution of Engineering and Technology

Adaptive active contours based on variable kernel with constant initialisation

ISSN 1751-9659
Received on 16th May 2017
Revised 20th January 2018
Accepted on 3rd February 2018
E-First on 6th March 2018
doi: 10.1049/iet-ipr.2017.0481
www.ietdl.org

Asad Munir[1], Shafiullah Soomro[1], Chang Ha Lee[1], Kwang Nam Choi[1] ✉

[1]*Department of Computer Science and Engineering, Chung-Ang University, Seoul 156-756, Korea*

✉ *E-mail: knchoi@cau.ac.kr*

Abstract: In this paper, a novel method of active contours based on the formulation of partial differential equation (PDE) is proposed for image segmentation. The evolution equation incorporates a force term that pushes the contour towards object boundary, a regularisation term which takes into account the smoothness of the level set function and an edge term which helps to stop the contour at required boundaries. The proposed method integrates an image convolved by a variable kernel into an energy formulation, where the width of the kernel varies in each iteration. Therefore, it takes local region information when the width of the kernel is small while for the larger width of the kernel, the proposed method considers global region information across the regions. Due to the use of both local and global image information, the method easily detects objects in the complex background and also segments the objects where intensity changes within the object. Moreover, the proposed method totally eliminates the need of the contour initialisation by using constant initialisation scheme. Experimental results on real and medical images prove the robustness of the proposed method. Finally, the authors validate their method on PH2 database for skin lesion segmentation.

1 Introduction

Image segmentation and boundary detection have a great importance in the fields of image analysis, pattern recognition and computer vision. The main purpose of image segmentation is to extract some required characteristics (object, a region of interest etc.) from the input image to make it simpler to analyse. Many successful image segmentation approaches and methodologies have been implemented using the level set method [1] involving partial differential equation (PDE) and the active contour methods [2–27].

An efficient active contour method is initially proposed by Kass *et al.* [2] for image segmentation, since then active contours have been widely used in image segmentation techniques. The primary idea of active contour methods is to deform a curve under the influence of PDE to detect the desired boundaries in an image.

On the basis of the image features used for segmentation, the existing active contour methods are divided into two categories: edge-based methods [4–10] and region-based methods [11–27]. Both of these two carry some advantages and drawbacks. Edge-based methods use image gradient information as an image based force to attract the contour towards the desired boundaries. These methods are very useful for the images having strong object boundaries and involve less computational complexities. However, these methods fail to detect the objects with weak and blurred boundaries. On the contrary, region-based methods [11–27] do not rely on the image gradient instead, these methods use the region-based statistical information inside and outside the contour within an image. These methods are also less sensitive to noise and can accurately segment the objects with the weak boundaries. Furthermore, these methods are less sensitive to the position of initial contour as well. One of the most typical and popular region-based methods is Chan–Vese method [11] which is based on the Mumford–Shah [22] segmentation technique. This method can well segment images with homogeneous intensity values across the regions because it considers that image intensity values are constant within each region of foreground and background. Therefore, this model does not provide satisfactory results in the presence of intensity inhomogeneity.

To overcome this problem, Li *et al.* [12] proposed the local binary fitting (LBF) model which is based on the local image information. This method deals well with intensity inhomogeneity by using Gaussian kernel inside the energy formulation. However, it has quite high computational time complexity and it is very sensitive to the position of the initial contour.

In 2012, Wang and He [23] proposed an adaptive level set evolution method which begins with a constant function. This method completely eliminates the need of contour initialisation and produce satisfying results on some synthetic and real images but it cannot deal properly with the images having intensity inhomogeneity.

Recently, Wen *et al.* [24] resolved the issue of intensity inhomogeneity in Wang and He's method [23] by using both local and global information of the image. This method used a weight variable to give the weights to local and global terms. This method can accurately detect the objects in inhomogeneous intensity. To find a suitable value for the weight variable manually is a problem in this method and it also fails when there is an intensity difference within the object to be detected.

Motivated by the Wang and He [23], Chan–Vese [11], LBF [12] and the Wen's methods [24], we propose an improved adaptive active contour method in the form of PDE. In this method, evolution equation is based on two terms: a force term which pulls the contour towards object boundaries and a regulation term which controls the smoothness of the level set function. The proposed method segment images having intensity variations within the object and the background by varying the width of the Gaussian kernel in each iteration. The force term is established by using region and edge information so that we can get the required results even in the presence of intensity inhomogeneity and blurred boundaries. Furthermore, our method completely eliminates the need of contour initialisation by initialising level set function to any bounded function (e.g. a constant function). By using the global and local terms alternatively, the issue of assigning the weight variable is solved. The Gaussian kernel plays an important role in this method as we convolve the image with the Gaussian kernel at every iteration to smooth the intensity variations within the objects which resolves the issue of detecting objects having intensity differences inside them. Experiment results on some real and medical images demonstrate the efficiency and robustness of our technique.

The rest of this paper is structured as follows. Section 2 briefly reviews some background and related methods. Section 3 presents the idea and formulation of the proposed method. Experimental results and comparisons are given in Section 4. Finally, some conclusions are drawn in Section 6.

2 Related work and background

2.1 Geodesic active contour (GAC) method

Let $I:[0,a]x[0,b] \to R^+$ is the given image and Ω is a bounded subset of R^2. In that bounded subset Ω, let $C(q):[0,1] \to R^2$ be a parameterised planer curve. Then GAC method [9] can be obtained by minimising the following energy function:

$$E^{GAC}(C) = \int_0^1 g(|\nabla I(C(q))|)|C'(q)|\,\mathrm{d}q \tag{1}$$

where g is an edge stopping function (ESF) defined as follows:

$$g(|\nabla I|) = \frac{1}{1+|\nabla G_\sigma * I|^2} \tag{2}$$

Minimisation of (1) by gradient descent method [28] gives us the following formulation:

$$C_t = g(|\nabla I|)\kappa \boldsymbol{N} - (\nabla g \cdot \boldsymbol{N})\boldsymbol{N} \tag{3}$$

where κ and $\boldsymbol{N}$ are the curvature and inward normal of the contour, respectively. Then the final level set equation can be written as follows:

$$\frac{\partial \phi}{\partial t} = g(|\nabla \phi|)\left(\mathrm{div}\left(\frac{\nabla \phi}{|\nabla \phi|}\right) + \alpha\right) + \nabla g \cdot \nabla \phi \tag{4}$$

where α is added to speed up the propagation and to control the shrinking or expanding of the contour.

2.2 Chan–Vese method

Chan–Vese [11] proposed an alternative solution to solve the issues in Mumford and Shah method [22]. For a given grey-level input image $I:\Omega \to R$ C is a closed curve, then the Chan–Vese formulation is explained as follows:

$$\begin{aligned} E^{\mathrm{CV}}(\mu, c_1, c_2) = {} & \mu L(C) + vA(in(C)) \\ & + \lambda_1 \int_\Omega |I(x) - c_1|^2 H_\varepsilon(\phi(x))\mathrm{d}x \\ & + \lambda_2 \int_\Omega |I(x) - c_2|^2 (1 - H_\varepsilon(\phi(x)))\mathrm{d}x \end{aligned} \tag{5}$$

where $\mu \geq 0$, $v \geq 0$ and $\lambda_1, \lambda_2 \geq 0$ are constants and $H(\phi)$ is regularised Heaviside function defined as

$$H_\varepsilon = \frac{1}{2}\left(1 + \frac{2}{\pi}\arctan\left(\frac{z}{\varepsilon}\right)\right) \tag{6}$$

The first term in (5) is the Euclidean length of the closed curve C and the second term indicates the area inside the curve C. c_1 and c_2 are the average values for image intensities inside and outside of moving curve C, respectively. By minimisation of above equation with respect to c_1 and c_2, we obtain following solutions:

$$c_1 = \frac{\int_\Omega I(x)H_\varepsilon(\phi(x))\mathrm{d}x}{\int_\Omega H_\varepsilon(\phi(x))\mathrm{d}x} \tag{7}$$

$$c_2 = \frac{\int_\Omega I(x)(1 - H_\varepsilon(\phi(x)))\mathrm{d}x}{\int_\Omega (1 - H_\varepsilon(\phi(x)))\mathrm{d}x} \tag{8}$$

By applying the gradient descent method [28], we can obtain the final PDE as follows:

$$\frac{\partial \phi}{\partial t} = \delta(\phi)\left[\mu \cdot \mathrm{div}\left(\frac{\nabla \phi}{|\nabla \phi|}\right) - v - \lambda_1 (I - c_1)^2 - \lambda_2 (I - c_2)^2\right] \tag{9}$$

μ and v are responsible for controlling smoothness and speed of level set function, respectively. $\delta(\phi)$ in above equation is a smooth version of Dirac delta function which is explained as

$$\delta_\varepsilon(z) = \frac{\varepsilon}{\pi(z^2 + \varepsilon^2)} \tag{10}$$

where epsilon controls the width of Dirac delta function.

Chan–Vese method [11] is less sensitive to the position of initial contour but this method gives poor segmentation results for the images with intensity inhomogeneity.

2.3 LBF model

To resolve the issue of intensity inhomogeneity, Li *et al.* [12] proposed the LBF model by utilising the local image information. The LBF model [12] can deal well with intensity inhomogeneity. The idea of this method is to introduce the kernel function to define the energy function as

$$\begin{aligned} E^{\mathrm{LBF}}(C, f_1, f_2) = {} & \lambda_1 \int \int_{\mathrm{inside}(C)} K_\sigma(x - y)|I(y) - f_1(x)|^2 \mathrm{d}y\mathrm{d}x \\ & + \lambda_2 \int \int_{\mathrm{outside}(C)} K_\sigma(x - y)|I(y) - f_2(x)|^2 \mathrm{d}y\mathrm{d}x \end{aligned} \tag{11}$$

where λ_1 , $\lambda_2 > 0$ are fixed parameters. K_δ is a Gaussian kernel having standard deviation σ. f_1 and f_2 are two smooth functions estimating the local image intensities inside and outside the contour C, respectively. These two functions are defined as

$$f_1(x) = \frac{K_\sigma \times [H_\varepsilon(\phi)I(x)]}{K_\sigma \times H_\varepsilon(\phi)} \tag{12}$$

$$f_2(x) = \frac{K_\sigma \times [1 - H_\varepsilon(\phi)I(x)]}{K_\sigma \times (1 - H_\varepsilon(\phi))} \tag{13}$$

For the Lipchitz function ϕ, the curve C is denoted by the zero level set, and with the minimisation of the energy functional E^{LBF}, we obtained the gradient descent flow as follows:

$$\frac{\partial \phi}{\partial t} = -\delta_\varepsilon(\phi)(\lambda_1 e_1 - \lambda_2 e_2) \tag{14}$$

where e_1 and e_2 are defined as

$$e_1 = \int K_\sigma(y - x)|I(x) - f_1(y)|^2 \mathrm{d}y \tag{15}$$

$$e_2 = \int K_\sigma(y - x)|I(x) - f_2(y)|^2 \mathrm{d}y \tag{16}$$

The LBF model [12] can accurately segment the images with intensity inhomogeneity due to the kernel function and local image information. However, the issue with this technique is that it is sensitive to the initialisation of the contour.

2.4 Wang and He's method

An adaptive level set evolution starting with a constant function is proposed by Wang and He [23]. The evolution equation is based on two forces: an adaptive force and a regularisation force to control the propagation speed and smoothness of the contour. The formulation of this approach in PDE framework on the level set function ϕ is defined as follows:

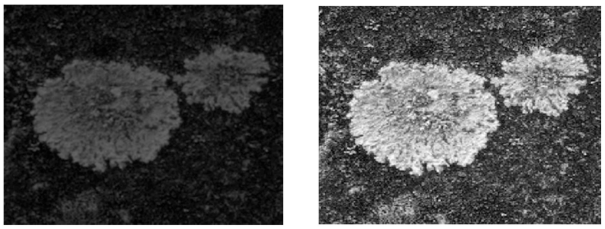

Fig. 1 *Applying different kernel width*
(a) Large kernel width, ***(b)*** Small kernel width

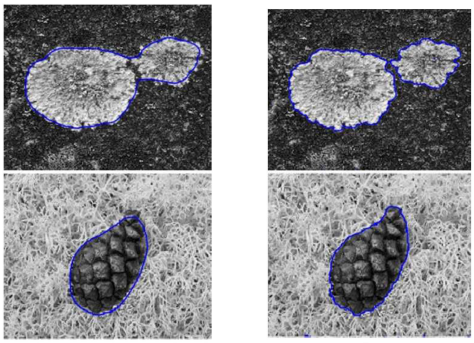

Fig. 2 *Role of ESF*
(a) Without applying ESF, ***(b)*** When ESF is introduced

$$\frac{\partial \phi}{\partial t} = g(|\nabla I_\sigma|)\left(\alpha f(I, c_1, c_2) + \beta \mathrm{div}\left(\frac{\nabla \phi}{|\nabla \phi|}\right)\right) \tag{17}$$

where α and β are the constants, α controls the evolution speed of the contour while β produces the effect on regularisation term for noise in the input image. c_1 and c_2 are the intensity values defined in (7) and (8), respectively. Adaptive force f is given as follows:

$$f(I, c_1, c_2) = \mathrm{sign}\left(I(x, y) - \frac{c_1 + c_2}{2}\right) \tag{18}$$

In this method, level set is simply initialised as a constant function that solves the problem of initialisation of the contour. This method cannot provide accurate results on the images with intensity inhomogeneity.

3 Proposed model

In this section, we propose a modified region-based active contour model in a PDE formulation based on the concept of Chan–Vese [11], LBF [12] and Wang and He's [23] methods. In this method, the zero level set curve segments the required object by using local and global intensity information alternatively.

For a given image $I: \Omega \subset R^2 \to R$, the suggested model is given as follows:

$$\frac{\partial \phi}{\partial t} = \alpha \cdot F(x, y, \phi) + \beta \cdot \Delta \phi \tag{19}$$

where $\alpha, \beta > 0$ are constants. The first term in (19) is an external force $F(x, y, \phi)$ and it pushes the contour towards the required object boundaries during the evolution process. The formulation of this force is defined as

$$F(x, y, \phi) = \mathrm{sign}\left(K(x, y) - \frac{v_1 + v_2}{2}\right) \tag{20}$$

v_1 and v_2 are image intensity values inside and outside of contour which are defined as

$$v_1 = \frac{\int_\Omega K(x, y) H_\varepsilon(\phi(x, y))\mathrm{d}x\mathrm{d}y}{\int_\Omega H_\varepsilon(\phi(x, y))\mathrm{d}x\mathrm{d}y} \tag{21}$$

$$v_2 = \frac{\int_\Omega K(x, y)[1 - H_\varepsilon(\phi(x, y))]\mathrm{d}x\mathrm{d}y}{\int_\Omega [1 - H_\varepsilon(\phi(x, y))]\mathrm{d}x\mathrm{d}y} \tag{22}$$

where $K(x, y)$ is convolved image with Gaussian kernel G, defined as

$$K(x, y) = G(x, y) * I(x, y) \tag{23}$$

The behaviour of the contour evolution is affected by force term in (19) as it holds different signs inside and outside the objects, so that if $F(x, y, \phi) > 0$, then $\partial\phi/\partial t > 0$, the level set function increases and if $F(x, y, \phi) < 0$, then $\partial\phi/\partial t < 0$, the level set function decreases. Therefore, the contour can move up or down adaptively, depending on an alternative sign of the force function. Due to the above-mentioned property of force term, the level set function ϕ can be initialised to any constant function which produces the zero level curve automatically. Therefore, any constant can be used as contour initialisation. $G(x, y)$ in (23) is a Gaussian kernel and its width varies in every iteration during the evolution process. $K(x, y)$ is the integration of convolved image with that variable kernel.

Kernel width plays a crucial role in image segmentation process. The reason for that is, when we convolve an image with large kernel width, it is not easy to describe the accurate boundary due to over-smoothing as it reduces the shape details as shown in Fig. 1*a*. On the other hand, for the too small kernel width, the result may contain multiple, irregular, bogus and blur boundaries as shown in Fig. 1*b*. In our method, we convolve the given input image with the spatial Gaussian kernel, where the width of the kernel σ increases from smaller to a larger value in the evolution process. Initially, when the kernel width is small the proposed method takes local intensity information across the regions and segment objects in the presence of intensity inhomogeneity. Similarly, for larger kernel width our method takes global region information and performs segmentation in homogenous regions.

The regularisation term in (19) for the smoothness of the zero level set and controlling the occurrence of infrequent small contours in the final segmentation can be written as

$$\Delta\phi = \partial^2\phi/\partial x^2 + \partial^2\phi/\partial y^2 \tag{24}$$

By using the advantage of edge-based models to avoid boundary leakage problem shown in Fig. 2*a*, we introduced an ESF in our method. With this ESF, the final level set equation can be rewritten as

$$\frac{\partial \phi}{\partial t} = g(\nabla I)[\alpha \cdot F(x, y, \phi) + \beta \cdot \Delta\phi] \tag{25}$$

where $g(\nabla I)$ is ESF which avoids the error in boundaries and leakage problem as shown in Fig. 2*b*.

An ESF $g(\nabla I)$ is taken from GAC model [9] and defined as

$$g(|\nabla I|) = \frac{1}{1 + |\nabla G_\sigma * I|^2} \tag{26}$$

Here G_σ is the same Gaussian kernel defined in (17) and its width σ varies in every iteration.

Our method completely eliminates the need of contour initialisation by using constant function initialisation technique adapted in Wang and He's [23] method.

The initial level set function with constant function is defined as

$$\phi_0(x, y) = \rho, \ (x, y) \in \Omega \tag{27}$$

where ρ is a positive constant (we use $\rho = 1$ for our method).

Finally, the main summary of the proposed method is shown in Fig. 3.

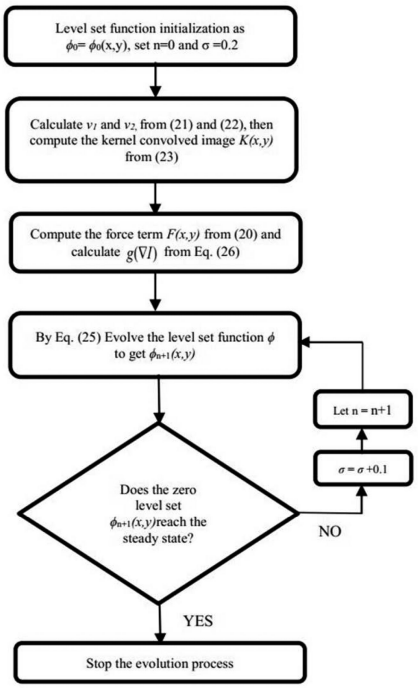

Fig. 3 *All steps to summarise the proposed algorithm*

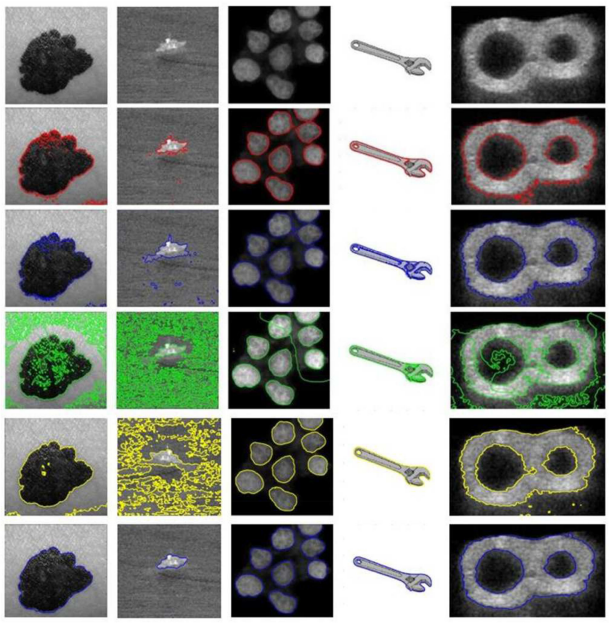

Fig. 4 *Results of our method for real images: (first row) original images; (second row) results of Chan-Vese model; (third row) results of Wang and He's model; (fourth row) results of LBF model; (fifth row) results of Wen's model; (last row) results of proposed model*

4 Experimental results

We have tested our method on a variety of real and medical images taken from different modalities with the following parameters $\alpha = 5$, $\beta = 0.2$, $\Delta T = 5$, $\varepsilon = 1.5$ and $\sigma = 0.2$. This is the initial value for δ as it increases in every iteration of the evolution process. The initial level set function is always chosen as a constant function, i.e. $\phi_0 = 1$. In all the experiments, we have compared our results with Chan–Vese method [11], LBF model [12], Wang and He's method [23] and Wen's method [24], respectively.

Fig. 4 illustrates the segmentation result of some real images with little fluctuations in the intensity. The first row shows the original images, the second row shows the result of the Chan–Vese method, third, fourth and fifth rows show the result of Wang and He's, LBF and Wen's methods, respectively. Sixth row results in the last row show that our method has successfully captured desired

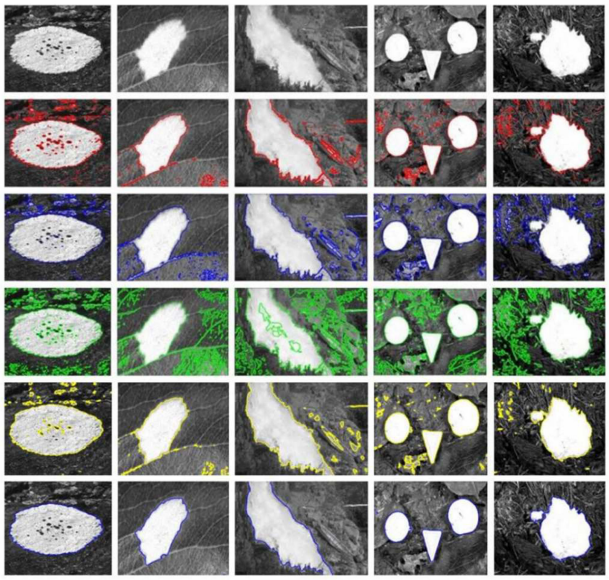

Fig. 5 *Results of Chan-Vese, Wang and He's, LBF and our methods for real images. The first row: original images. The second row: results of Chan-Vese model. The third row: results of Wang and He's model. The fourth row: results of LBF model. The fifth row: results of Wen's model and the sixth row: results of our model*

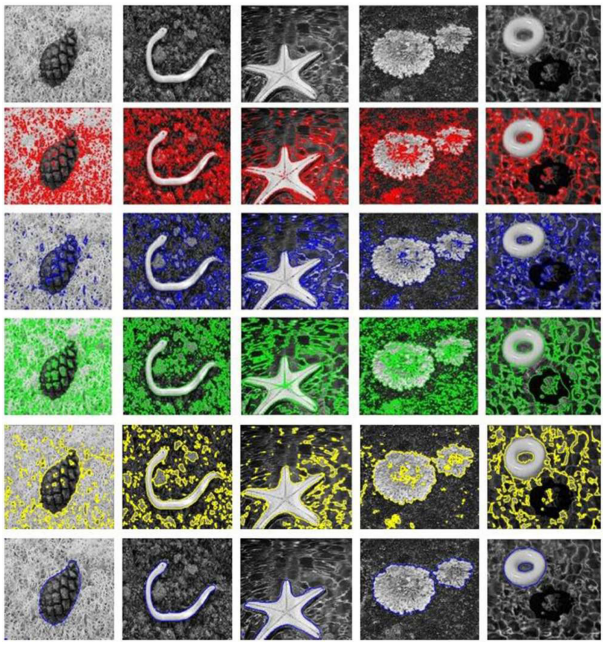

Fig. 6 *Segmentation results of four models for real images. The first row: original images; the second to fifth rows: segmentation results of Chan-Vese, Wang and He's, LBF, Wen's and ours, respectively*

segmentation where the previous methods have failed to segment required objects.

In Fig. 5, some more results with real images having some complex background taken from Science Photo Library (https://www.sciencephoto.com) have been shown. The first row consists of original images and the other rows show results for Chan–Vese method [11], Wang and He's method [23], LBF method [12], Wen's method [24] and our method from top to bottom, respectively.

In all previous methods, the contour is also segmenting the background with the object as all these images have intensity varying background but our method can precisely detect these objects in the given images.

Figs. 6 describes this method for some more real images with much complex backgrounds also taken from Science Photo Library (https://www.sciencephoto.com) and comparison with the other four methods.

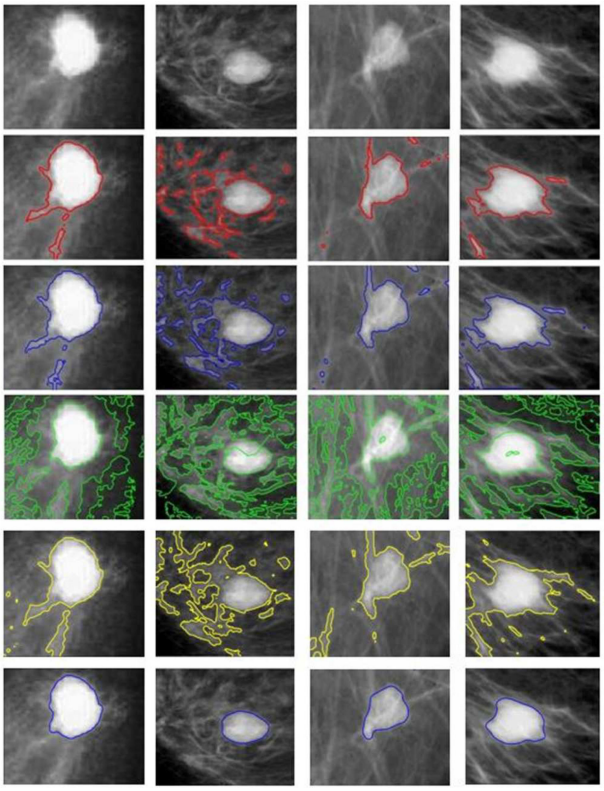

Fig. 7 *Segmentation results of four models for digital mammography images. The first row: original images; the second to fifth rows: segmentation results of Chan-Vese, Wang and He's, LBF, Wen's and ours, respectively*

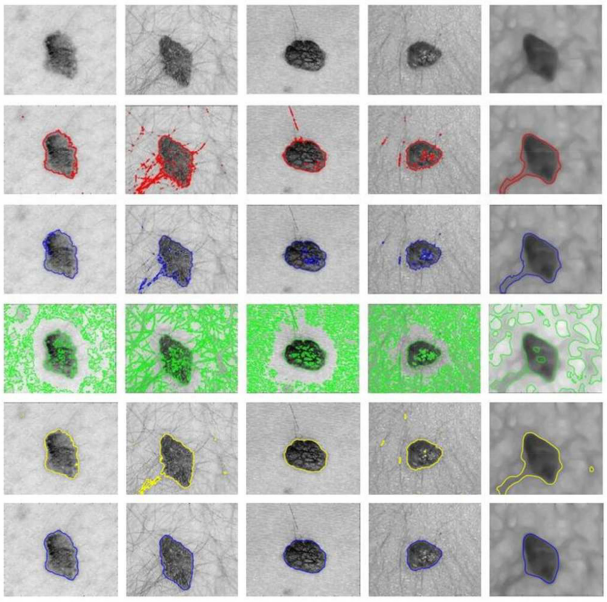

Fig. 8 *Segmentation results of four models for skin lesion images taken from Photo Science Library: (top row) original images; (second row) results of Chan-Vese model; (third row) results of Wang and He's model; (fourth row) results of LBF model; (fifth row) results of Wen's model; (bottom row) results of the proposed model*

The contour just scattered in the whole image due to the existence of complex background in all images. First and fourth columns in Fig. 6 have the images where the intensity changes within the required object and all the three methods completely failed to detect the object as the contour is also detecting many other intensity changes within the required object. The results prove that this technique can easily overcome the problem of intensity variations within the object and complex background.

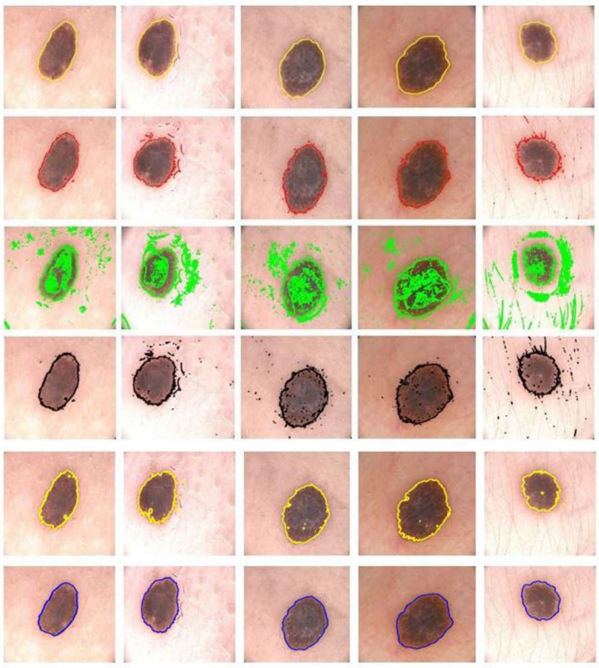

Fig. 9 *Segmentation results of four models for skin lesion images taken from PH2 database: (top row) original images; (second row) results of Chan-Vese model; (third row) results of Wang and He's model; (fourth row) results of LBF model; (fifth row) results of Wen's model; (bottom row) results of the proposed model*

Fig. 7 shows the comparison of our method with other four methods for segmentation of tumours in real digital mammography images. Typically, the tumours are brighter than the background in mammography images. However, some tumours have similar intensities with their background and have blurred boundaries. As shown in Fig. 7, all the other methods failed to extract the object boundary properly. On the other hand, our method has accurately segmented the required region of interest compared to the previous methods.

4.1 Application in skin lesion segmentation

Over the past few decades, the rate of skin cancer has been increasing continuously and its deadliest form is Melanoma [29]. To increase the survival rate, early detection and proper treatment are very crucial. Therefore, many imaging techniques have been developed to detect the melanoma. In the recent years, Barata *et al.* [30], Riaz *et al.* [31], Barata *et al.* [32] and Yao *et al.* [29] proposed several methods to improve the accuracy for detecting the melanoma. The proposed method has higher accuracy and better performance than the previous methods in the segmentation of melanoma. We have used Science Photo Library (https://www.sciencephoto.com) and PH2 database [33] to test our method on different dermoscopic images.

Figs. 8 and 9 show the segmentation results of the proposed method for real skin lesion images taken from Science Photo Library and PH2 database [30], respectively. The primary step in computer-aided lesion analysis is to extract the lesion region from the background. However, it is very difficult to find the accurate segmentation results due to the complex background and obscure boundaries. The first row contains the original images and ground truths in Figs. 8 and 9, respectively. The second row shows the results for Chan–Vese method, third and fourth rows give the segmentation results of Wang *et al.* method and LBF method and the last row shows the results for the proposed method, respectively. These segmentation results for skin lesion images prove that our method is more accurate as compared to other three methods.

Fig. 10 shows the segmentation result of our method with respect to the ground truth on some images taken form PH2 database [30]. The red contour is ground truth and the blue contour

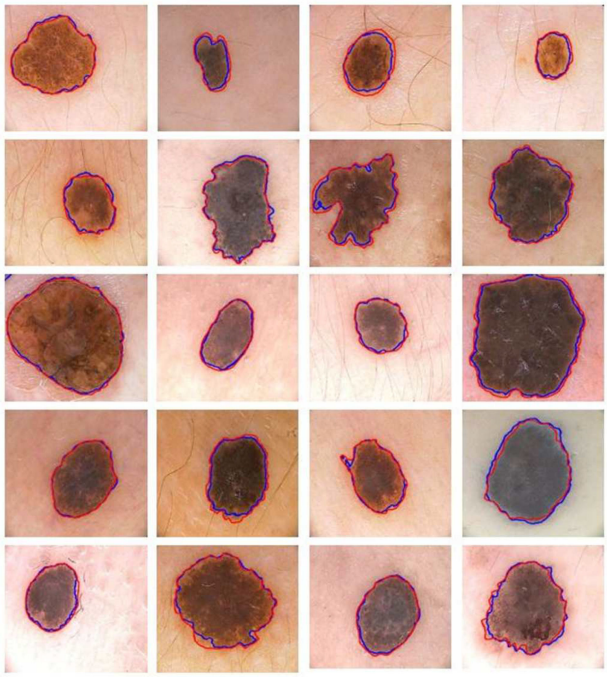

Fig. 10 *Segmentation results of the proposed model for images from PH2 database: red contour shows the ground truth and blue contour shows the results of the proposed model*

is the result of the proposed method. These results prove that our method well segmented the required melanoma in these images almost same as the ground truth.

5 Discussion

5.1 Robustness of the proposed method

Results on real and medical images show the strength of the proposed method. First, second and last columns of Fig. 4 have the images with smooth background and blur boundaries where proposed method provides satisfying results for them. Third and fourth columns of Fig. 5 and second, third and fifth columns of Fig. 6 show the validity of this method on images having the complex background and all other methods failed to detect the required object as they segment many things in the background as well. The first column of Fig. 5 and first and fourth columns in Fig. 6 have the images with intensity variation exits inside the objects. Other four methods are having a contour inside the object due to this intensity variation while proposed method works very accurately on these images. So the proposed method gives satisfying results in the presence of blur boundaries, complex background and intensity variations inside the object.

5.2 Contour initialisation

The effect of contour initialisation on segmentation results is entirely eliminated as the level set function ϕ simply initialised to a constant function $\phi_0(x,y) = \rho > 0$, as explained in (27). The large value of ρ gradually decreases the rate of convergence of the zero level set. So for faster convergence rate ρ should have a smaller value. A value between 0 and 5 provides satisfactory performance with the proposed algorithm.

5.3 Time step

A large time step is used in the numerical implementation of this method. As the time step controls the speed of evolution so larger time step can speed up the algorithm but may cause boundary leakage problem if the time step is too large. Similarly, if the time step is too small then the algorithm takes too much time to converge to the required boundaries. Time step between 1 and 10 works properly in the proposed model. In our experiments, we use time step $\Delta T = 5$ to obtain the required segmentation results.

Table 1 Comparison with different methods on PH2 database

Methods	Sensitivity, %	Specificity, %	Accuracy, %
Barata *et al.* [30]	98	79	89
Riaz *et al.* [31]	84	94	89
Barata *et al.* [32]	98	90	94
Yao *et al.* [29]	95	98	97
proposed	93.1	99.3	97.6

5.4 Evaluation of PH2 database

In Table 1, we compared the sensitivity, specificity and accuracy of the proposed method with recent four proposed methods on PH2 database. The sensitivity shows that without taking false positives into account whether obtained information has the same information what we need

$$\text{Sensitivity} = \frac{\text{TP}}{\text{TP} + \text{FN}}$$

The specificity shows how correctly the true negative region is ignored during segmentation

$$\text{Specificity} = \frac{\text{TN}}{\text{TN} + \text{FP}}$$

Accuracy term tells us the overall accuracy of the segmentation result across the whole image domain

$$\text{Accuracy} = \frac{(\text{TN} + \text{TP})}{(\text{TP} + \text{FP} + \text{TN} + \text{FN})}$$

Our method has best specificity and accuracy among all these methods and in the case of sensitivity, our method has better performance than Riaz [31]. Overall, the proposed method has an acceptable performance in skin lesion segmentation.

6 Conclusion

This paper presents a region-based active contour model for image segmentation by using PDE formulation which controls the contour evolution by a force term and a regularisation term. Due to the varying kernel width in every evolution step, the proposed method behaves as local region based model initially and as the kernel width increase it acts as a global region based model.

An ESF is also used with same varying kernel width which stops the contour at the required boundaries efficiently. Moreover, the need of initial contour is completely eliminated by using initialising the level set function to any constant function. The change of kernel width gives flexibility to the proposed method to act as local and global alternatively. Due to which it accurately segments the images in the presence of intensity differences inside the object as well as images with blurred boundaries and complex background.

Experimental results prove that the proposed algorithm yields better segmentation results on many real and medical images. Furthermore, comparison results with the other methods verify the robustness of our technique.

7 Acknowledgment

This research was supported by Basic Science Research Program through the National Research Foundation of Korea (NRF), funded by Ministry of Education, Science, and Technology (NRF-2010-0025512).

8 References

[1] Osher, S., Sethian, J.A.: 'Fronts propagating with curvature-dependent speed: algorithms based on hamilton-jacobi formulations', *J. Comput. Phys.*, 1988, **79**, (1), pp. 12–49

[2] Kass, M., Witkin, A., Terzopoulos, D.: 'Snakes: active contour models', *Int. J. Comput. Vis.*, 1988, **1**, (4), pp. 321–331

[3] Hussain, S., Chun, Q., Asif, M.R., *et al.*: 'Active contours for image segmentation using complex domain-based approach', *IET Image Process.*, 2016, **10**, (2), pp. 121–129

[4] Goldenberg, R., Kimmel, R.: 'Fast geodesic active contours', *IEEE Trans. Image Process.*, 2001, **10**, (10), pp. 1467–1475

[5] Caselles, V., Catte, F., Coll, T., *et al.*: 'A geometric model for active contours in image processing', *Numer. Math.*, 1993, **66**, (1), pp. 1–31

[6] Chunming, L., Chenyang, X., Changfeng, G., *et al.*: 'Level Set evolution without Re-initialization: A New variational formulation'. IEEE Computer Society Conf. on Computer Vision and Pattern Recognition, June 2005, vol. 1, pp. 430–436

[7] Zhao, P., Ren, H.E., Pu, Z.B.: 'Simultaneous surface area measurement for multiple objects by geodesic active contour', *Optik – Int. J. Light Electron Optics*, 2009, **120**, (10), pp. 484–489

[8] Chunming, L., Chenyang, X., Changfeng, G., *et al.*: 'Distance regularized level set evolution and its application to image segmentation', *IEEE Trans. Image Process.*, 2010, **19**, (12), pp. 3243–3254

[9] Caselles, V., Kimmel, R., Sapiro, G.: 'Geodesic active contours', *Int. J. Comput. Vis.*, 1997, **22**, (1), pp. 61–79

[10] Kim, J.H., Park, B.Y., Akram, F., *et al.*: 'Multipass active contours for an adaptive contour map', *Sensors*, 2013, **13**, (3), pp. 3724–3738

[11] Chan, T.F., Vese, L.A.: 'Active contours without edges', *IEEE Trans. Image Process.*, 2001, **10**, (2), pp. 266–277

[12] Li, C., Kao, C.Y., Gore, J.C., *et al.*: 'Minimization of region-scalable fitting energy for image segmentation', *IEEE Trans. Image Process.*, 2008, **17**, (10), pp. 1940–1949

[13] Wang, L., Li, C., Sun, Q., *et al.*: 'Active contours driven by local and global intensity fitting energy with application to brain MR image segmentation', *Comput. Med. Imaging Graph.*, 2009, **33**, (7), pp. 520–531

[14] Vese, L.A., Chan, T.F.: 'A multiphase level set framework for image segmentation using the Mumford and Shah model', *Int. J. Comput. Vis.*, 2002, **50**, (3), pp. 271–293

[15] Zhang, K., Zhang, L., Song, H., *et al.*: 'Active contours with selective local or global segmentation: A new formulation and level set method', *Image Vis. Comput.*, 2010, **28**, (4), pp. 668–676

[16] Lankton, S., Tannenbaum, A.: 'Localizing region-based active contours', *IEEE Trans. Image Process.*, 2008, **17**, (11), pp. 2029–2039

[17] Peng, Y., Liu, F., Liu, S.: 'Active contours driven by normalized local image fitting energy', *Concurrency Comput. Pract. Exp.*, 2014, **26**, (5), pp. 1200–1214

[18] Wang, H., Huang, T.Z.: 'Region-based object and background extraction via active contours', *Optik – Int. J. Light and Electron Optics*, 2013, **124**, (23), pp. 6020–6026

[19] Jiang, X., Li, B., Wang, Q., *et al.*: 'A novel active contour model driven by local and global intensity fitting energies', *Optik – Int. J. Light and Electron Optics*, 2014, **125**, (21), pp. 6445–6449

[20] Soomro, S., Akram, F., Kim, J.H., *et al.*: 'Active contours using additive local and global intensity fitting models for intensity inhomogeneous image segmentation', *Comput. Math. Methods Med.*, 2016, **2016**, pp. 1–15

[21] El-Rewaidy, H., Ibrahim, E.S., Fahmy, A.S.: 'Segmentation of the right ventricle in MRI images using a dual active shape model', *IET Image Process.*, 2016, **10**, (10), pp. 717–723

[22] Mumford, D., Shah, J.: 'Optimal approximations by piecewise smooth functions and associated variational problems', *Commun. Pure Appl. Math.*, 1989, **42**, (5), pp. 577–685

[23] Wang, Y., He, C.: 'Adaptive level set evolution starting with a constant function'. *Appl. Math. Model.*, 2012, **36**, (7), pp. 3217–3228

[24] Wen, W.: 'Adaptive active contours based on local and global intensity information for image segmentation', *Optik-Int. J. Light and Electron Optics*, 2014, **125**, (23), pp. 6995–7001

[25] Akram, F., Garcia, M.A., Puig, D.: 'Active contours driven by local and global fitted image models for image segmentation robust to intensity inhomogeneity', *PloS one*, 2017, **12**, (4), pp. 1–34

[26] Zhang, L., Peng, X., Li, G., *et al.*: 'A novel active contour model for image segmentation using local and global region-based information', *Mach. Vis. Appl.*, 2017, **28**, (1-2), pp. 75–89

[27] Soomro, S., Akram, F., Munir, A., *et al.*: 'Segmentation of left and right ventricles in cardiac MRI using active contours', *Comput. Math. Methods Med.*, 2017, **2017**, pp. 1–16

[28] Aubert, G., Kornprobst, P.: '*Mathematical problems in image processing: partial differential equations and the calculus of variations*' (Springer-Verlag, New York, 2006, 2nd edn.), 147

[29] Yao, T., Wang, Z., Xie, Z., *et al.*: 'A multiview joint sparse representation with discriminative dictionary for melanoma detection'. Int. Conf. on Digital Image Computing: Techniques and Applications (DICTA), November 2016, pp. 1–6

[30] Barata, C., Ruela, M., Francisco, M., *et al.*: 'Two systems for the detection of melanomas in dermoscopy images using texture and color features', *IEEE Syst. J.*, 2014, **8**, (3), pp. 965–979

[31] Riaz, F., Hassan, A., Javed, M.Y., *et al.*: 'Detecting melanoma in dermoscopy images using scale adaptive local binary patterns'. 36th Annual Int. Conf. of the IEEE Engineering in Medicine and Biology Society, August 2014, pp. 6758–6761

[32] Barata, C., Celebi, M.E., Marques, J.S.: 'Melanoma detection algorithm based on feature fusion'. 37th Annual Int. Conf. of the IEEE Engineering in Medicine and Biology Society (EMBC), August 2015, pp. 2653–2656

[33] Mendonça, T., Ferreira, P.M., Marques, J.S., *et al.*: 'PH 2-A dermoscopic image database for research and benchmarking'. 35th Annual Int. Conf. of the IEEE Engineering in Medicine and Biology Society (EMBC), July 2013, pp. 5437–5440